The Astrophysical Journal, 604:687–692, 2004 April 1

LARGE-SCALE COSMIC-RAY ANISOTROPY WITH KASCADE

T. Antoni,[1] W. D. Apel,[2] A. F. Badea,[2,3] K. Bekk,[2] A. Bercuci,[2,3] H. Blümer,[1,2] H. Bozdog,[2] I. M. Brancus,[4] C. Büttner,[1] K. Daumiller,[1] P. Doll,[2] R. Engel,[2] J. Engler,[2] F. Fessler,[2] H. J. Gils,[2] R. Glasstetter,[1,5] A. Haungs,[2] D. Heck,[2] J. R. Hörandel,[1] K.-H. Kampert,[1,2,5] H. O. Klages,[2] G. Maier,[2,] H. J. Mathes,[2] H. J. Mayer,[2] J. Milke,[2] M. Müller,[2] R. Obenland,[2] J. Oehlschläger,[2] S. Ostapchenko,[1,6] M. Petcu,[4] H. Rebel,[2] A. Risse,[7] M. Risse,[2] M. Roth,[1] G. Schatz,[2] H. Schieler,[2] J. Scholz,[2] T. Thouw,[2] H. Ulrich,[2] J. van Buren,[2] A. Vardanyan,[8] A. Weindl,[2] J. Wochele,[2] and J. Zabierowski[7]
(The KASCADE Collaboration)
Received 2003 November 11; accepted 2003 December 15

ABSTRACT

We present the results of an analysis of the large-scale anisotropy of cosmic rays in the PeV range. The Rayleigh formalism is applied to the right ascension distribution of extensive air showers measured by the KASCADE (Karlsruhe Shower Core and Array Detector) experiment. The data set contains about 10^8 extensive air showers in the energy range 0.7–6 PeV. No hints of anisotropy are visible in the right ascension distributions in this energy range. This accounts for all showers, as well as for subsets containing showers induced by predominantly light or heavy primary particles, respectively. Upper flux limits for Rayleigh amplitudes are determined to be between 10^{-3} at a primary energy of 0.7 PeV and 10^{-2} at 6 PeV.

Subject heading: cosmic rays

On-line material: color figure

1. INTRODUCTION

The arrival direction of charged cosmic rays with primary energies between several hundred TeV and 10 PeV is remarkably isotropic. A possible anisotropy would reflect the general pattern of propagation of cosmic rays in the Galactic environment. Model calculations, e.g., those of Candia, Mollerach, & Roulet (2003), show that diffusion of cosmic rays in the Galactic magnetic field can result in an anisotropy on a scale of 10^{-4} to 10^{-2}, depending on particle energy and the strength and structure of the Galactic magnetic field. The diffusion is rigidity dependent; the cited model calculation reports an anisotropy that is roughly a factor of 5–10 larger for protons than for iron primary particles with the same energy. This rigidity-dependent diffusion is one of several explanations for the steepening in the cosmic-ray energy spectrum at ~4 PeV. Another class of models explains this so-called "knee" in the energy spectrum as a result of a change in the acceleration efficiency of the source (e.g., Lagage & Cesarsky 1983). There is no change in anisotropy at the knee expected from these models, while the models based on diffusion should result in an increase at ~4 PeV. Anisotropy measurements give, in addition to the measurements of mass-dependent energy spectra, valuable information for the discrimination between models that explain the knee in the cosmic-ray energy spectrum.

Because of the small anisotropy expected, a large data sample is necessary. The flux of cosmic rays in the PeV energy range is too low for direct measurement by experiments on satellites or balloons. Ground-based experiments with large collecting areas measuring the secondary products of the interaction of the primary cosmic rays with Earth's atmosphere are currently the only way to collect a suitable number of events. Few statistically significant anisotropies were reported from extensive air shower experiments in the last two decades. The EAS-TOP collaboration (Aglietta et al. 1996) published an amplitude of $(3.7 \pm 0.6) \times 10^{-4}$ at $E_0 \approx 200$ TeV. The Akeno experiment (Kifune et al. 1986) reported results of $\sim 2 \times 10^{-3}$ at ~5–10 PeV. An overview of experimental results can be found in Clay, McDonough, & Smith (1997).

In the following, the large-scale cosmic-ray anisotropy is studied by application of the Rayleigh formalism to data of the KASCADE (Karlsruhe Shower Core and Array Detector) air shower experiment. The two-dimensional distribution of the arrival directions of cosmic rays is reduced to one coordinate because of the limited field of view and the small amplitudes expected from theory and previous observations. A first-order approximation of the multipole expansion of the arrival directions of cosmic rays is a harmonic analysis of the right ascension values of extensive air showers. The Rayleigh formalism gives the amplitude A and phase Φ of the first harmonic, and, in addition, the probability P for detecting a spurious amplitude due to fluctuations from a sample of n events that are drawn from a uniform distribution (Mardia & Jupp 1999):

$$A = \sqrt{C^2 + S^2}, \quad \Phi = \arctan\frac{S}{C}, \tag{1}$$

[1] Institut für Experimentelle Kernphysik, Universität Karlsruhe, 76021 Karlsruhe, Germany.
[2] Institut für Kernphysik, Forschungszentrum Karlsruhe, 76021 Karlsruhe, Germany; gernot.maier@ik.fzk.de.
[3] On leave of absence from the National Institute of Physics and Nuclear Engineering, 7690 Bucharest, Romania.
[4] National Institute of Physics and Nuclear Engineering, 7690 Bucharest, Romania.
[5] Current address: Universität Wuppertal, 42119 Wuppertal, Germany.
[6] On leave of absence from Moscow State University, 119899 Moscow, Russia.
[7] Soltan Institute for Nuclear Studies, 90950 Lodz, Poland.
[8] Cosmic Ray Division, Yerevan Physics Institute, Yerevan 36, Armenia.

$$S = \frac{2}{n}\sum_{i=1}^{n} \sin\alpha_i, \quad C = \frac{2}{n}\sum_{i=1}^{n} \cos\alpha_i, \tag{2}$$

$$P(>A) = \exp(-nA^2/4) + O(n^{-2}). \tag{3}$$

The sum includes n right ascension values α_i.

Studies of higher harmonics are very limited, as the expected amplitudes are too small compared to the statistical fluctuations of the data sets available.

In this article, an analysis of data from the KASCADE experiment is presented, which is described in the following section. The data selection procedures, including an enrichment of light and heavy primary particles, are presented in § 3 and § 4. In § 5, we describe the corrections applied to the shower rates depending on atmospheric ground pressure and temperature. The main results, i.e., the Rayleigh amplitudes for all showers as well as for the mass-enriched samples, can be found in § 6.

2. KASCADE: EXPERIMENTAL SETUP AND DATA RECONSTRUCTION

The extensive air shower experiment KASCADE is located at Forschungszentrum Karlsruhe, Germany (E8.°4, N49.°1), at 110 m above sea level, corresponding to an average vertical atmospheric depth of 1022 g cm^{-2}. KASCADE measures the electromagnetic, muonic, and hadronic components of air showers with three major detector systems: a large field array, a muon tracking detector, and a central detector (Antoni et al. 2003a).

In the present analysis, data from the 200×200 m^2 scintillation detector array are used. The 252 detector stations are uniformly spaced on a square grid, with 13 m between each station. The grid is organized into squares of 4×4 stations to form electronically independent clusters, with 16 stations in the 12 outer clusters and 15 stations in the four inner clusters. The stations in the inner and outer clusters contain four or two liquid scintillator detectors, respectively, covering a total area of 490 m^2. In addition, plastic scintillators are mounted below an absorber of 10 cm of lead and 4 cm of iron in the 192 stations of the outer clusters (622 m^2 total area). The absorber corresponds to 20 electromagnetic radiations lengths, entailing a threshold for vertical muons of 230 MeV. This configuration allows measurement of the electromagnetic and muonic components of extensive air showers. The number of electrons (N_e) and muons (N_μ) in a shower, the position of the shower core, and the shower direction are determined in an iterative shower-reconstruction procedure. The "truncated" muon number ($N_{\mu,\mathrm{tr}}$) denotes the number of muons in the distance range 40–200 m from the shower core. Shower directions are determined without assuming a fixed geometrical shape of the shower front, by evaluating the arrival times of the first particle in each detector and the total particle number per station. The angular resolution for zenith angles less than 40° is 0.°55 for small showers and 0.°1 for showers with electron numbers of $\log_{10} N_e \geq 6$.

The detector array reaches full detection efficiency for extensive air showers with electron numbers $\log_{10} N_e > 4$, corresponding to a primary energy of $\sim(6-9) \times 10^{14}$ eV. This is defined by a detector multiplicity condition that results in a trigger rate of ~3 Hz. The data set for the following analysis contains 10^8 events recorded in 1600 days between 1998 May and 2002 October.

3. DATA SELECTION

Because of the very small amplitudes expected, a very careful data selection is necessary. Contributions from amplitudes in local solar time can cause spurious signals in sidereal time. This leakage is due to the very small difference in day length between a solar and a sidereal day ($\Delta t = 236$ s). Amplitudes in solar time can be caused by variation of atmospheric ground pressure and temperature, and are corrected for (§ 5). To minimize these spurious effects, several cuts are applied to the measured showers in order to enhance data quality. In the following, rates are determined in time intervals of half an hour (which in sidereal time ≈1795 s). In detail, the selection criteria are as follows:

1. To ensure reconstruction quality, only showers well inside the detector field, with a maximum distance to its center of 91 m and with zenith angles smaller than 40°, have been used. The latter cut restricts the visible sky to the declination band $9^\circ < \delta < 89^\circ$.
2. More than 249 of the 252 detector stations have to be in working condition.
3. Sudden changes in the rate are detected by testing the uniformity of the rate as a function of time for each sidereal day. No deviations of the rates from the mean rate larger than 4 σ, determined over the whole measurement time, are allowed.
4. Only sidereal days with continuous data taking are used.
5. The array has to be fully efficient (100%) for extensive air shower (EAS) detection. Simulations show that this is the case for electron numbers $\log_{10} N_e > 4$.

After application of these quality cuts, about 20% of the showers from the initial data set remain. In total, 269 of 1622 sidereal days with continuous data taking are used in the following analysis. The seasonal distribution of these days is as follows: 114 days in spring (February–April), 18 in summer (May–July), 77 in autumn (August–October), and 60 in winter (November–January).

4. ENRICHMENT OF LIGHT AND HEAVY PRIMARIES

To evaluate the dependence of a possible Rayleigh amplitude on primary energy and mass, the data set is divided by a simple cut of the $\log_{10} N_{\mu,\mathrm{tr}} - \log_{10} N_e$ plane into two sets. Simulation studies show that showers initiated by light primary particles are predominately electron-rich, while those from heavy primaries are electron-poor (Antoni et al. 2002). The EASs are simulated utilizing the CORSIKA package (Heck et al. 1998). The QGSJET model (Kalmykov, Ostapchenko, & Pavlov 1997) is used for hadronic interactions above $E_{\mathrm{Lab}} > 80$ GeV, and the GHEISHA model (Fesefeldt 1985) is used for interactions below this energy. The electromagnetic cascades are simulated by EGS4 (Nelson, Hirayama, & Rogers 1985). The shower simulation is followed by a detector simulation based on GEANT.[9] A power law with constant spectral index of $\gamma = -2$ is used in the simulations. Figure 1 shows the distribution of muon number versus electron number ($\log_{10} N^0_{\mu,\mathrm{tr}}$ vs. $\log_{10} N^0_e$) of showers measured with KASCADE and from the above-mentioned simulations of proton- and iron-induced showers. There are several reasons for the differences between the measured and the simulated distributions: the chemical composition of cosmic rays consists of more than two components,

[9] GEANT 3.21, Detector Description and Simulation Tool, see CERN Program Library Long Writeup W5015, Application Software Group.

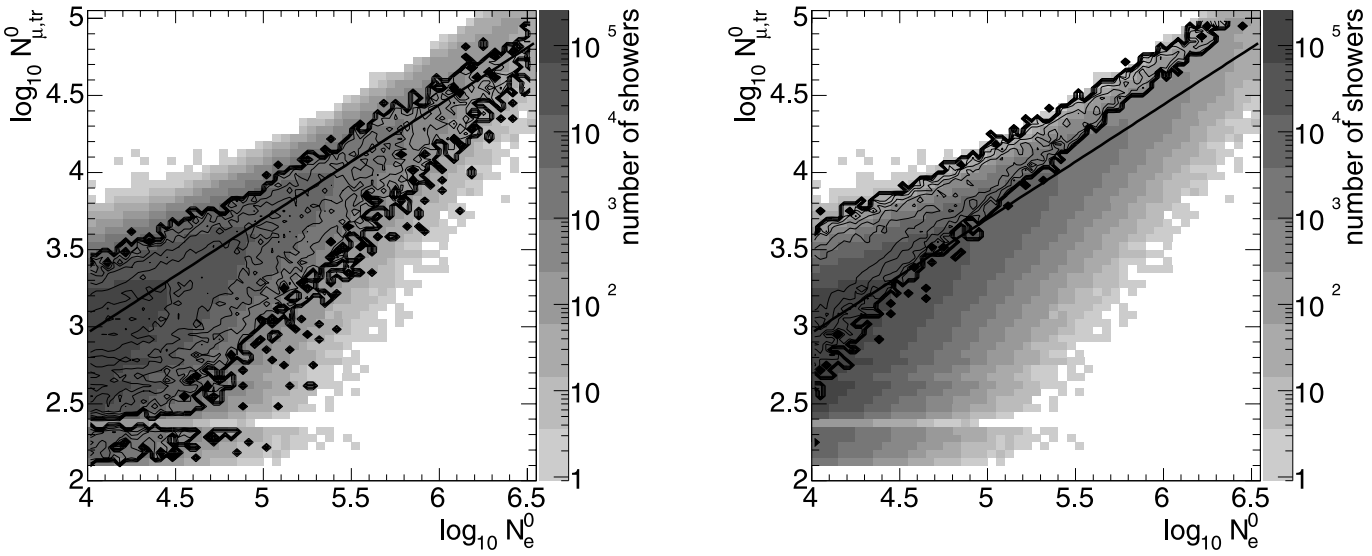

FIG. 1.—Number of muons vs. number of electrons ($\log_{10} N^0_{\mu,\mathrm{tr}}$ vs. $\log_{10} N^0_e$) for showers measured with KASCADE (*shaded area*). Plots of simulated air showers induced by primary protons (*left*) or iron nuclei (*right*) are superposed (*contour lines*). The straight lines in both figures indicate the separation between light and heavy primaries according to eq. (4). [*See the electronic edition of the Journal for a color version of this figure.*]

the slope of the energy spectrum of the cosmic rays is different in the simulations, and the number of measured showers exceeds by far the number of simulated showers.

A separation between light and heavy primaries can be expressed by the ratio

$$\log_{10} N^0_{\mu,\mathrm{tr}} / \log_{10} N^0_e = 0.74. \tag{4}$$

The electron number N_e and the truncated muon number $N_{\mu,\mathrm{tr}}$ are zenith-angle corrected to $\Theta = 0^\circ$ using the attenuation law

$$N^0_e = N_e \exp[X_0/\Lambda_e(\sec\Theta - 1)], \tag{5}$$

$$N^0_{\mu,\mathrm{tr}} = N_{\mu,\mathrm{tr}} \exp\left[X_0/\Lambda_{\mu,\mathrm{tr}}(\sec\Theta - 1)\right], \tag{6}$$

with the attenuation lengths $\Lambda_{N_e} = 175$ g cm^{-2} and $\Lambda_{N_{\mu,\mathrm{tr}}} = 823$ g cm^{-2} (Antoni et al. 2003b).

This separation neglects the large fluctuations, especially of proton-initiated showers. It also neglects the very different relative abundances of light to heavy primaries in cosmic rays.

5. CORRECTION FOR ATMOSPHERIC GROUND PRESSURE AND TEMPERATURE

The influence of the atmospheric ground pressure P and temperature T on the rate of extensive air showers at ground level is taken into account by a second-order polynomial with additional time-dependent corrections ΔR_i for i different configurations of the detector system (e.g., with slightly different high voltages of the detectors),

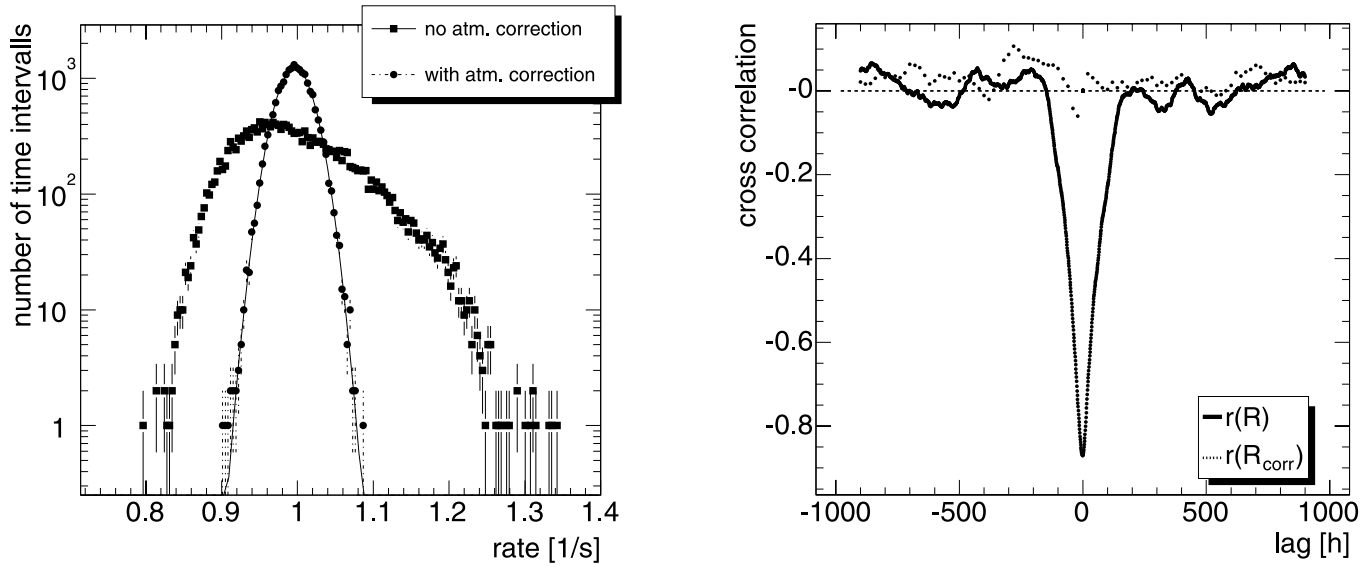

FIG. 2.—*Left*: Distribution of rates with and without correction for atmospheric ground pressure and temperature. A fit by a Gaussian function is shown by the line. *Right*: Cross correlation between hourly shower rate and atmospheric ground pressure with $[r(R_{\mathrm{corr}})]$ and without $[r(R)]$ atmospheric correction.

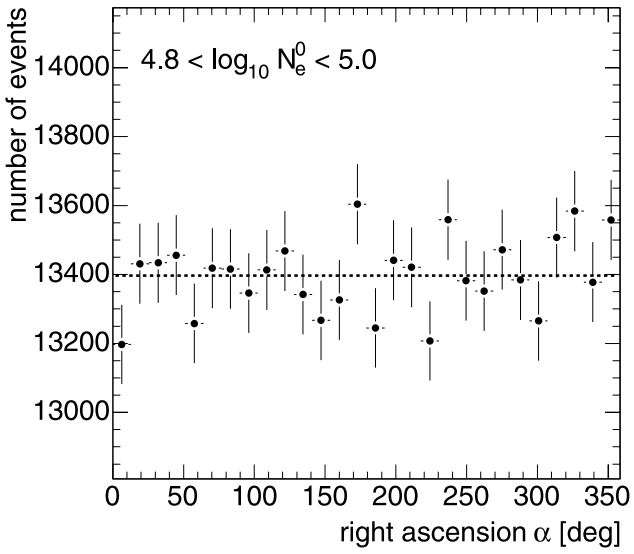

FIG. 3.—Example of a right ascension distribution after correction for atmospheric ground pressure and temperature in the stated electron number interval. The dashed line reflects the mean number of events.

$$R(P,T,i) = R_0 + \Delta R_i + p_1(P-P_0) + p_2(P-P_0)^2 + p_3(T-T_0) + p_4(T-T_0)^2 + p_5(P-P_0)(T-T_0). \quad (7)$$

The detector parameters are constant during each of the i time intervals. $R_0 = 0.966\ \mathrm{s}^{-1}$, $P_0 = 1002.95$ hPa, and $T_0 = 9.7^\circ$C are the long-time mean values of rate, ground pressure, and temperature. All parameters p_{1-5} and ΔR_i are estimated by a fit to the time-dependent rates for the whole interval of 4 yr and result in $p_1 = (-7.21 \pm 0.0016) \times 10^{-3}$, $p_2 = (-3.00 \pm 0.13) \times 10^{-5}$, $p_3 = (-3.64 \pm 0.0023) \times 10^{-3}$, $p_4 = (-3.19 \pm 0.22) \times 10^{-5}$, and $p_5 = (-3.76 \pm 0.253) \times 10^{-5}$ in units of hPa, °C, and s. The values for the ΔR_i are between -2×10^{-2} and 2×10^{-2} s^{-1}. The correction itself is done for time intervals of 1795 s by subtracting or adding the necessary number of events calculated by equation (7). Events are chosen randomly from the half-hour intervals to lower the number of showers. The events that have to be added for this correction are chosen randomly from the set of showers of the same sidereal day. The quality of the correction can be estimated from Figure 2. The left figure shows the event-rate distributions before and after the corrections. The uncorrected rates reflect the asymmetric distribution of the atmospheric ground pressure. The distribution of the corrected rates is compatible with a Gaussian distribution, which is expected from remaining statistical fluctuations of the event rate. The right figure shows the cross correlation between rate and ground pressure. The very strong correlation $r(R)$ visible for the uncorrected rates vanishes after the correction $r(R_{\mathrm{corr}})$ with equation (7).

6. RESULTS

An example of the right ascension distributions of showers after atmospheric correction for electron numbers in the interval $4.8 < \log_{10} N_e^0 < 5$ is shown in Figure 3. The Rayleigh amplitudes A of the right ascension distributions for electron numbers in the range $\log_{10} N_e^0 = 4 - 6.6$ are calculated according to equation (1).

The lower electron number limit is the efficiency threshold of the KASCADE detector field. As mentioned in § 3, full efficiency is required in order to minimize effects of the threshold to the amplitudes. The upper electron number limit at $\log_{10} N_e^0 = 6.6$ is determined by the small number of events (≈1000) in this electron number interval.

The showers are sorted in intervals of electron number $\log_{10} N_e^0$ and not in intervals of truncated muon number $\log_{10} N_{\mu,\mathrm{tr}}^0$, although the latter is a better estimator for primary energy and less dependent on the mass of the primary particle. The trigger threshold of the detector field is mainly determined

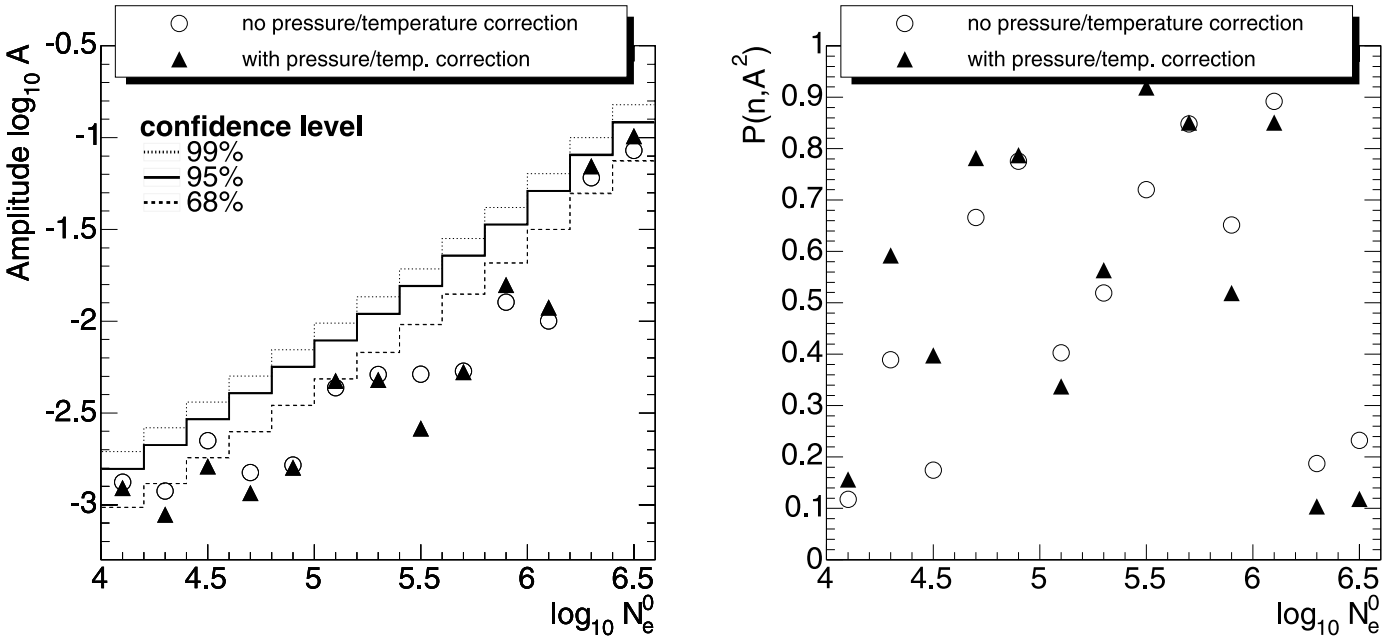

FIG. 4.—Results from the Rayleigh analysis for showers with and without correction for atmospheric ground pressure and temperature. *Left*: Rayleigh amplitude A vs. electron number $\log_{10} N_e^0$. *Right*: Probability $P(n, A^2)$ that the amplitudes plotted in the left figure are fluctuations from underlying uniform distributions.

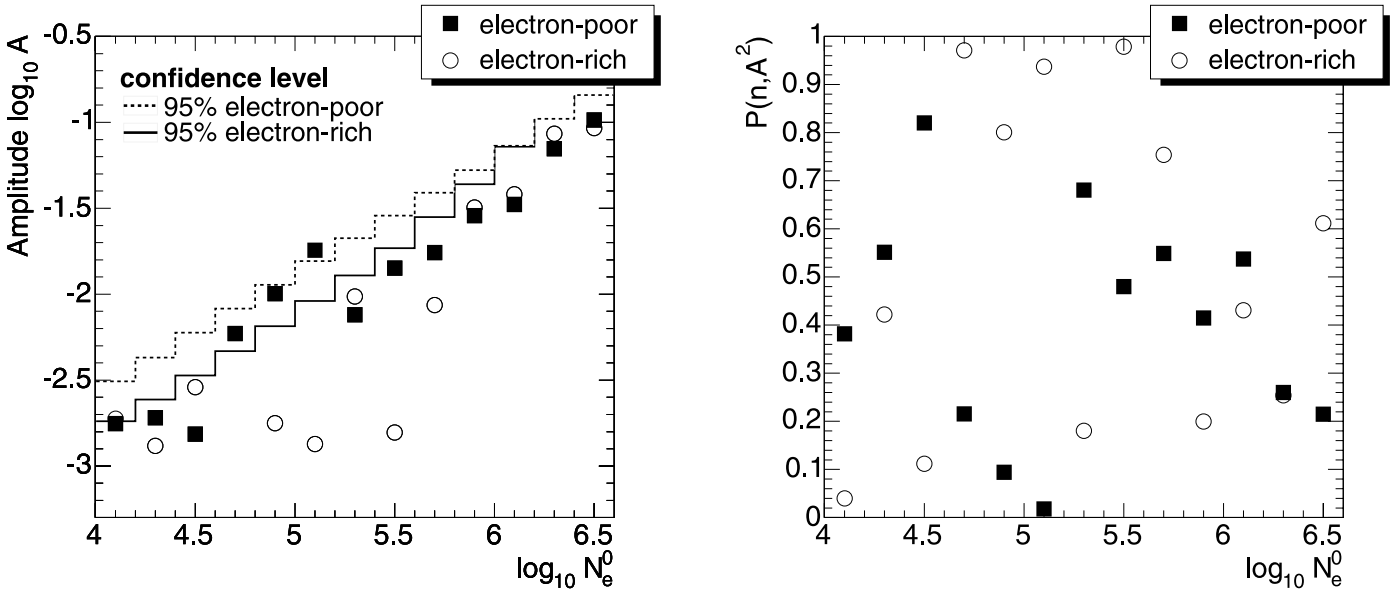

FIG. 5.—Results from the Rayleigh analysis for data sets of predominately light and heavy primaries. *Left*: Rayleigh amplitude A vs. electron number $\log_{10} N_e^0$. *Right*: Probability $P(n, A^2)$ that the amplitudes in the left figure are fluctuations from underlying uniform distributions.

by the number of electrons. The usage of $N_{\mu,\mathrm{tr}}^0$ combined with the requirement of full detection efficiency would shift the lower energy threshold of this analysis to energies above 4×10^{15} eV.

Figure 4 (*left*) shows the resulting Rayleigh amplitudes. The lines indicate the confidence levels for Rayleigh amplitudes with probabilities $1 - P(> A)$ of 68%, 95%, and 99%, respectively. Assuming a power law with spectral index γ for the form of the electron-size spectrum, the confidence levels are also power laws with spectral indices of $-\gamma/2$ (see eq. [3]). The confidence levels are only a function of the number of events used in the analysis. Therefore, the increase of the confidence levels with electron number by no means reflects an increase of anisotropy. Amplitudes that are below the lines indicating the confidence levels can be treated as fluctuations and are of no physical meaning. All calculated amplitudes are well below the 95% line. The fluctuation probability $P(> A)$ of each Rayleigh amplitude is shown in Figure 4 (*right*). The probabilities are all above 5%. There are no hints of nonzero Rayleigh amplitudes within the statistical limits.

The results of the two subsets of data containing electron-rich and electron-poor showers are shown in Figure 5. No correction for ground pressure P and temperature T is applied in this case. In addition to altering the detection rate, the variations of P and T also alter the number of electrons and muons in a shower, and therefore alter the effect of the separation line (eq. [4]) between electron-poor and electron-rich showers. A further correction would require detailed information about the influence of atmospheric variations on N_e and $N_{\mu,\mathrm{tr}}$, which is beyond the scope of this analysis. Only a detection of significant amplitudes would require such additional steps. As can be seen from Figure 5, no anisotropy can be deduced from the calculated amplitudes and fluctuation probabilities. The most prominent amplitude at $5 < \log_{10} N_e^0 < 5.2$ has a significance of $\sigma = 2.2$. The intersection of the confidence levels of electron-poor and electron-rich showers is due to the increasing fraction of heavy primary cosmic rays with increasing primary energy in the region of the knee (Antoni et al. 2002).

In addition to the results presented in Figures 4 and 5, an analysis of the data set with different definitions of the electron number intervals, and for showers above the knee sorted by truncated muon numbers, yielded the same result of no significant amplitudes.

Figure 6 shows the upper limits on the large-scale anisotropy derived in this analysis, in context with results from other experiments and predictions from the model of Candia et al. (2003). The primary energies of the extensive air showers measured by KASCADE are determined by a linear

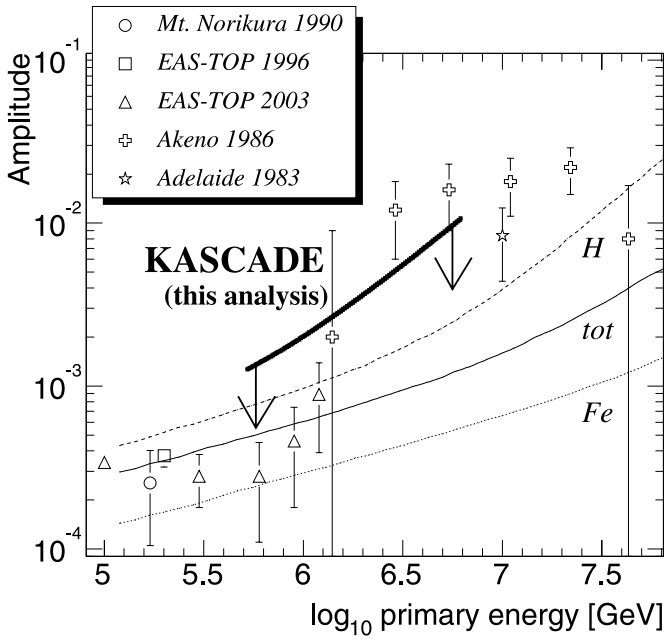

FIG. 6.—KASCADE upper limits (95%) of Rayleigh amplitudes A vs. primary energy (*thick line*) compared to reported results from the literature (Nagashima et al. 1990; Aglietta et al. 1996, 2003; Kifune et al. 1986; Gerhardy & Clay 1983). Model predictions from Candia et al. (2003) for the total anisotropy and for the anisotropies of the proton and iron components are also shown (*thin lines*).

transformation of the particle numbers $\log_{10} N_e^0$ and $\log_{10} N_{\mu,\mathrm{tr}}^0$. The transformation matrix is determined from CORSIKA simulations using the hadronic interaction models QGSJET and GHEISHA. The uncertainty of this simplified primary energy determination is about 20%. The figure shows that the KASCADE upper limits are in the range of the reported results from other experiments. The EAS-TOP experiment reported somewhat lower limits in the energy range below 2×10^{15} eV. The relatively large amplitudes published by the Akeno experiment are difficult to reconcile with the results of this analysis. The model calculations, which are of course dependent on parameters such as the source distribution and the strength and structure of the Galactic magnetic field, yield amplitudes in the range of 3×10^{-4} to 2×10^{-3} in the energy range of KASCADE. This is about a factor of 4–10 lower than the upper limits derived in this analysis. The contribution of anisotropy measurements toward a solution of the enigma of the knee are therefore still small. A significant observation of the anisotropy of separate cosmic-ray components around and above the knee requires much larger data sets compared to those currently available.

The authors would like to thank the members of the engineering and technical staff of the KASCADE collaboration who contributed with enthusiasm and commitment to the success of the experiment. The KASCADE experiment is supported by the German Federal Ministry of Education and Research and was embedded in collaborative WTZ projects between Germany and Romania (RUM 97/014), Poland (POL 99/005), and Armenia (ARM 98/002). The Polish group acknowledges support by KBN grant 5PO3B 13320.

REFERENCES

Aglietta, M., et al. 1996, ApJ, 470, 501
———. 2003, Proc. 28th Int. Cosmic Ray Conf. (Tsukuba), 4, 183
Antoni, T., et al. 2002, Astropart. Phys., 16, 373
———. 2003a, Nucl. Instrum. Methods Phys. Res. A, 513, 490
———. 2003b, Astropart. Phys., 19, 703
Candia, J., Mollerach, S., & Roulet, E. 2003, J. Cosmol. Astropart. Phys., 5, 3
Clay, R., McDonough, M.-A., & Smith, A. 1997, Proc. 25th Int. Cosmic Ray Conf. (Durban), 4, 185
Fesefeldt, H. 1985, The Simulation of Hadronic Showers: Physics and Applications (Geneva: CERN)
Gerhardy, P., & Clay, R. 1983, J. Phys. G, 9, 1279
Heck, D., Knapp, J., Capdevielle, J. N., Schatz, G., & Thouw, T. 1998, CORSIKA: A Monte Carlo Code to Simulate Extensive Air Showers (Karlsruhe: Forschungszentrum Karlsruhe)
Kalmykov, N. N., Ostapchenko, S. S., & Pavlov, A. I. 1997, Nucl. Phys. B Proc. Suppl., 52, 17
Kifune, T., et al. 1986, J. Phys. G, 12, 129
Lagage, P., & Cesarsky, C. 1983, A&A, 118, 223
Mardia, V., & Jupp, P. 1999, Directional Statistics (New York: Wiley)
Nagashima, K., et al. 1990, Proc. 21st Int. Cosmic Ray Conf. (Adelaide), 3, 180
Nelson, W. R., Hirayama, H., & Rogers, D. W. O. 1985, The EGS4 Code System, SLAC 265 (Stanford: Stanford Univ.)